Electronic structure of $PrCoO_3$ and its temperature evolution

S. K. Pandey, Swapnil Patil, V. R. R. Medicherla, R. S. Singh, and Kalobaran Maiti*
Department of Condensed Matter Physics and Materials Science, Tata Institute of Fundamental Research, Homi Bhabha Road, Colaba, Mumbai 400 005, India

(Received 3 November 2007; revised manuscript received 25 January 2008; published 27 March 2008)

We investigate the detailed electronic structure of $PrCoO_3$ and its temperature evolution by using high-resolution photoemission spectroscopy and *ab initio* band structure calculations. We observe that, in addition to the correlation effect, spin-orbit interaction plays an important role in determining the electronic properties of this system. Pr $4f$ states are found to be strongly hybridized with the O $2p$ and Co $3d$ valence electronic states and appear in the vicinity of the Fermi level. The calculated results corresponding to the intermediate spin state of Co provide a good representation of the experimental spectra at 300 K. The decrease in temperature from 300 K leads to a gradual enhancement of the O $2p$ character in the bonding features, indicating the signature of an enhancement of the low spin state contributions at lower temperatures. The temperature evolution of the shift of the valence band edge is found to be consistent with the transport data.

DOI: 10.1103/PhysRevB.77.115137 PACS number(s): 71.20.−b, 71.27.+a, 75.20.Hr, 79.60.Bm

I. INTRODUCTION

Cobaltates with general formula $ACoO_3$ ($A \equiv$ rare-earth ions) form an interesting class of compounds in the perovskite family.[1] The primary concern in these systems is the understanding of the temperature induced spin state transition. Extensive effort has been put forward both theoretically and experimentally to understand this effect. The ground state of these compounds is believed to be a nonmagnetic (spin $S=0$) insulator having a Co^{3+} ion in low spin (LS) configuration; all the six $3d$ electrons occupy the Co t_{2g} band. An increase in temperature leads to two magnetic transitions accompanied by an insulator to metal transition in the vicinity of the second transition temperature.[2–6] It was suggested that the magnetic transitions occur due to the thermally driven spin state transition of Co^{3+} ions.[7–9] The major controversy in these studies involves the identification of the spin state in the intermediate temperature range. Some studies[9–18] suggest that the spin state of Co is an intermediate spin (IS $\Rightarrow t_{2g\uparrow}^3 e_{g\uparrow}^1 t_{2g\downarrow}^2$; $S=1$) state, while the others suggest a mixed low spin and high spin (HS $\Rightarrow t_{2g\uparrow}^3 e_{g\uparrow}^2 t_{2g\downarrow}^1$; $S=2$) state.[7,8,19–23] Despite numerous investigations on this issue, the controversy in the spin state transition is still unresolved.

Most of the studies mentioned above have focused on the spin state transitions in $LaCoO_3$, where the crystal field splitting is close to the exchange interaction strength. If we replace La with Pr, the smaller ionic radius of Pr as compared to that of La provides a chemical pressure on the system. It is observed that the crystal structure of $PrCoO_3$ is orthorhombic, while that of $LaCoO_3$ is rhombohedral.[6,12] The average Co-O bond length of $PrCoO_3$ is less than that of $LaCoO_3$. Thus, the crystal field splitting is expected to be enhanced in $PrCoO_3$ as compared to that in $LaCoO_3$. The Co-O-Co bond angle in $PrCoO_3$ is smaller than that in $LaCoO_3$. In addition, $4f$ electrons corresponding to Pr atoms and the hybridization of the $4f$ states with the valence electronic states will play an important role in determining the magnetic properties in this system.

The transport and optical conductivity measurements exhibit a larger band gap and a higher insulator to metal transition temperature in $PrCoO_3$ as compared to those in $LaCoO_3$.[4] It was suggested that the decrease in valence band width due to the change in Co-O-Co bond angle leads to such effect. The temperature dependent infrared spectroscopy data of $PrCoO_3$ showed the LS to IS state transition at around 220 K.[16] The susceptibility data of $PrCoO_3$ obtained after subtracting the contributions from Pr^{3+} ions showed increased population of the IS state at around 200 K.[17] Thus, $PrCoO_3$ is an ideal system to throw some light in understanding the interplay between crystal field splitting and exchange coupling strength in the spin state transition in cobaltates.

In the present work, we investigate the temperature evolution of the spin state of a Co ion in $PrCoO_3$ by using high-resolution photoemission spectroscopy and *ab initio* band structure calculations. The experimental valence band spectra exhibit the signature of a gradual increase in band gap with a decrease in temperature. The comparison of the experimental and calculated results for the valence band indicates that the Co ion presumably possesses a dominant IS state configuration in the temperature range of 150–300 K. This is also manifested in the shallow core level spectra. Spin-orbit coupling (SOC) plays an important role in determining the electronic structure in this system.

II. EXPERIMENTAL AND COMPUTATIONAL DETAILS

$PrCoO_3$ was prepared in the polycrystalline form by a combustion method.[24] Nitrates of Pr and Co were taken in appropriate amount and mixed in double distilled water. In this mixture, 2 moles of glycine per mole of metal cation were added and stirred until all of the compounds dissolved in the water. The resulting solution was slowly heated at a temperature around 200 °C until all of the water evaporated. The precursor thus formed catches fire on its own, turning into the powder of the compound. The hard pellets of this powder were formed and heated at 1200 °C for one day. The sample was characterized by x-ray powder diffraction and resistivity measurements. The powder diffraction data did not show any impurity peak; all the peaks were well fitted with on orthorhombic phase (space group *Pbnm*) by using

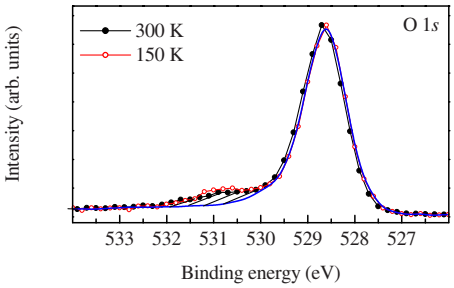

FIG. 1. (Color online) O 1*s* core level spectra recorded at 300 K (solid circles) and 150 K (hollow circles). The shaded region shows the impurity contributions.

the Rietveld refinement technique. The lattice parameters obtained from the fitting match well with those reported in the literature. Resistivity data are also consistent with the available data in the literature.[4,6]

The photoemission spectra were recorded by using a spectrometer equipped with monochromatic sources such as Al $K\alpha$ (1486.6 eV), ultraviolet sources, He II (40.8 eV), and He I (21.2 eV). The electron detection was carried out by a Gammadata Scienta analyzer SES2002. The energy resolution for the x-ray photoemission (XP) was set to 0.3 eV for the valence band and 0.6 eV for the core level spectra. The energy resolution for the He II and He I spectra were fixed to 4.2 and 1.4 meV, respectively. The base pressure during the measurements was about 4×10^{-11} Torr. We have used a He cryostat, LT-3M from Advanced Research Systems for the measurements at different temperatures.

The sample was cleaned *in situ* by scraping the sample surface using a diamond file. The cleanliness of the sample was ascertained by tracking the sharpness of the O 1*s* peak and the absence of the C 1*s* peak. The O 1*s* spectra recorded at 150 and 300 K are shown in Fig. 1. The contribution of an impurity peak at around 531 eV binding energy is negligible ($<3\%$), indicating the good quality of the sample. The Fermi level was aligned by recording the valence band spectrum of a Ag foil mounted on the same sample holder.

The generalized gradient approximation (GGA) and GGA+U (U=the electron correlation strength) calculations were carried out by using LMTART 6.61.[25] To calculate the charge density, a full-potential linearized muffin-tin orbital method working in plane wave representation was employed. In the calculation, we have used the muffin-tin radii of 3.43, 2.019, and 1.688 a.u. for Pr, Co, and O, respectively. The charge density and effective potential were expanded in spherical harmonics up to l=6 inside the sphere and in a Fourier series in the interstitial region. The initial basis set included 6*s*, 5*p*, 5*d*, and 4*f* valence and 5*s* semicore orbitals of Pr; 4*s*, 4*p*, and 3*d* valence and 3*p* semicore orbitals of Co; and 2*s* and 2*p* valence orbitals of O. The exchange correlation functional of the density functional theory was taken after Vosko *et al.*,[26] and GGA was implemented by using the prescription of Perdew *et al.*[27] The effect of spin-orbit coupling was also considered in the calculations.

In the GGA+U calculations, the Hubbard U and exchange J were considered as parameters. Since the valency of Co is close to 3+ in both $LaCoO_3$ and $PrCoO_3$, and it is

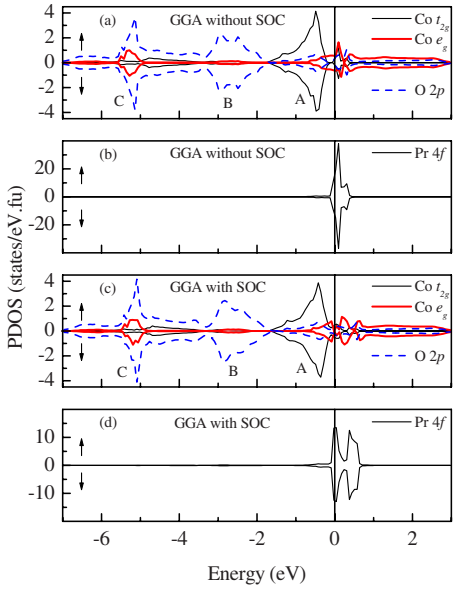

FIG. 2. (Color online) (a) O 2*p* (dashed line) and Co 3*d* partial density of states having t_{2g} (thin solid line) and e_g (thick solid line) symmetries. (b) Pr 4*f* partial density of states obtained from GGA calculation. (c) O 2*p* (dashed line) and Co 3*d* partial density of states having t_{2g} (thin solid line) and e_g (thick solid line) symmetries. (d) Pr 4*f* partial density of states obtained from GGA calculation including SOC.

well known that the on-site Coulomb correlation remains almost the same in such cases,[28,29] we have fixed U_{dd} =3.5 eV and J=1.0 eV for Co 3*d* electrons following the literature.[30,31] U_{ff} for Pr 4*f* electrons was varied from 3.5 to 5.5 eV. We have not considered the value of J for Pr 4*f* electrons exclusively in the calculations. It is estimated under GGA formulation. Calculations were performed by taking LS, IS, and HS configurations, which correspond to $(t^3_{2g\uparrow}t^3_{2g\downarrow})$, $(t^3_{2g\uparrow}t^2_{2g\downarrow}e^1_{g\uparrow})$, and $(t^3_{2g\uparrow}t^1_{2g\downarrow}e^2_{g\uparrow})$ electronic configurations, respectively, as initial input. It is already well known that in contrast to the standard GGA, there are several stable solutions corresponding to different local minima of the GGA+U functional. Thus, a different starting spin configuration leads to the lowest energy solution of the corresponding spin state. The convergence in total energy was set to 10^{-4} Ryd/cell. Final orbital occupancies for Pr 4*f* and Co t_{2g} and e_g states were obtained from self-consistent GGA+U calculations for different initial state configurations. (8, 8, 6) divisions of the Brillouin zone along three directions for the tetrahedron integration were used to calculate the density of states (DOS).

III. RESULTS AND DISCUSSIONS

Co t_{2g}, Co e_g, and O 2*p* partial density of states (PDOS) obtained from GGA calculations are plotted in Fig. 2(a) and PDOS of Pr 4*f* in Fig. 2(b). It is evident from the figures that there are finite PDOSs of Co e_g, O 2*p*, and Pr 4*f* at the Fermi level, indicating the metallic ground state, which is in contrary to the experimentally observed insulating ground state. The PDOS below the Fermi level can be divided into three

regions: (i) region A up to −1.6 eV from the Fermi level, (ii) region B from −1.6 to −3.4 eV, and (iii) region C below −3.4 eV. Region A has a dominating Co 3*d* character along with small O 2*p* contributions having a similar energy distribution of the PDOS. This feature is attributed to the antibonding states. The Co 3*d* states having t_{2g} symmetry appear between −1.6 and −0.2 eV and the contribution of Co 3*d* states having e_g symmetry appear between −0.5 and 2.5 eV. Region B is essentially contributed by the nonbonding O 2*p* states. The bonding states having t_{2g} and e_g symmetries contribute in region C with a dominant contribution from O 2*p* electronic states. The contribution of Pr 4*f* PDOS appears in the narrow region from −0.1 to 0.4 eV, indicating the highly localized nature of Pr 4*f* electrons.

In order to investigate the role of spin-orbit coupling in the electronic structure in the limit of generalized gradient approximations, we have calculated the density of states including SOC. The calculated PDOSs of Co t_{2g}, Co e_g, and O 2*p* states are shown in Fig. 2(c) and that of Pr 4*f* states in Fig. 2(d). It is clear from the figure that the inclusion of SOC has negligible influence on the Co 3*d* and O 2*p* PDOSs. However, SOC drastically modifies the Pr 4*f* PDOS, as is evident from Fig. 2(d). It splits into two well separated regions. The region below 0.25 eV is identified to be due to Pr $4f_{5/2}$ states and the region above 0.25 eV appears due to Pr $4f_{7/2}$ contributions. The spin-orbit splitting of Pr 4*f* states is found to be about 0.4 eV.

It is clear from Fig. 2 that the DOS at the Fermi level, ϵ_F, is finite in both cases (with SOC and without SOC), which is an indication of a metallic ground state. Thus, the consideration of electron correlation is necessary to capture the insulating ground state observed experimentally.

The inclusion of on-site Coulomb correlation on Co 3*d* electrons (U_{dd}=3.5 eV) under GGA+*U* formulation modifies the positions and distributions of Co 3*d* and O 2*p* PDOSs as is evident in Fig. 3(a). The most significant effect of U_{dd} is observed in the antibonding Co t_{2g} states (the feature A in the figure), which shift to lower energy by about 0.8 eV. The contribution of the O 2*p* states is significantly enhanced in this energy range. As expected, U_{dd} does not affect Pr 4*f* bands. Interestingly, Co e_g states have a finite contribution at the Fermi level, which is not expected as the inclusion of U_{dd} of 3.5 eV was sufficient to create a hard gap of about 0.22 eV in $LaCoO_3$.[30] This indicates that Pr 4*f* states strongly hybridize with the O 2*p* and Co e_g orbitals in the vicinity of the Fermi level. This is also manifested by the shape of the energy distribution of the DOS in this energy region. Still, there is finite DOS at ϵ_F, characterizing the system to be metallic.

In order to capture the correct ground state of $PrCoO_3$, we have included the on-site Coulomb correlation among Pr 4*f* electrons (U_{ff}). Since the *f* electrons are more localized than the *d* electrons, the electron correlation strength among *f* electrons is expected to be larger than that for *d* electrons. Thus, U_{ff}=U_{dd}=3.5 eV can be taken as a good approximation for the lower limit of U_{ff}. We have varied U_{ff} from 3.5 to 5.5 eV to achieve the best representation of the experimental spectra. As will be shown later, we find that U_{ff} =3.5 eV provides the best representation of the experimental 4*f* feature. In Fig. 3(c), we show the Co t_{2g}, Co e_g, and O 2*p*

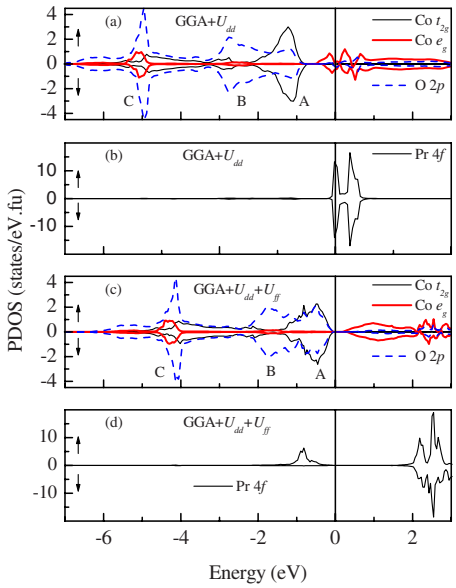

FIG. 3. (Color online) (a) O 2*p* (dashed line) and Co 3*d* partial density of states having t_{2g} (thin solid line) and e_g (thick solid line) symmetries and (b) Pr 4*f* partial density of states obtained from GGA+*U* calculation when on-site Coulomb correlation between Co 3*d* electrons is considered. (c) O 2*p* (dashed line) and Co 3*d* partial density of states having t_{2g} (thin solid line) and e_g (thick solid line) symmetries and (d) Pr 4*f* partial density of states obtained from GGA calculation when on-site Coulomb correlation between Co 3*d* and Pr 4*f* electrons is considered. In all the calculations, SOC is included.

PDOSs. The Pr 4*f* PDOSs obtained are shown in Fig. 3(d). The Pr 4*f* PDOSs exhibit a large splitting, leading to a large energy gap of 2.2 eV between the occupied and unoccupied bands. Interestingly, such a splitting introduces a significant modification in the Co 3*d* and O 2*p* DOSs. The 4*f* symmetry adapted Co 3*d* and O 2*p* states also appear in the same energy range as that of the 4*f* bands and a band gap of 0.27 eV appears between the t_{2g} and e_g states, characterizing the system to be an insulator.

In addition, the inclusion of U_{ff} introduces a large shift of features A, B, and C toward the Fermi level along with a significant change in the energy separation among themselves. While feature A is predominantly contributed by Co 3*d* PDOS in Fig. 3(a), the contribution from O 2*p* PDOS to feature A is significantly, enhanced making it almost equal to that from the Co 3*d* state. It is thus evident that Pr 4*f* states play an important role in determining the electronic states in the vicinity of ϵ_F and, hence, the electronic properties of this system.

We now study the effect of the different spin configurations of the Co^{3+} ion on the valence band calculated by using GGA+*U* method. The Pr 4*f*, Co 3*d*, and O 2*p* PDOSs corresponding to Co^{3+} ion in LS, IS, and HS configurations are plotted in Figs. 4(a)–4(c), respectively. It is evident from the figure that the insulating gap of about 0.27 eV observed for the LS configuration is not present in the other cases. In addition, there are several changes in the valence band corresponding to the IS and HS states as compared to that for the LS state. The low energy spread of the valence band

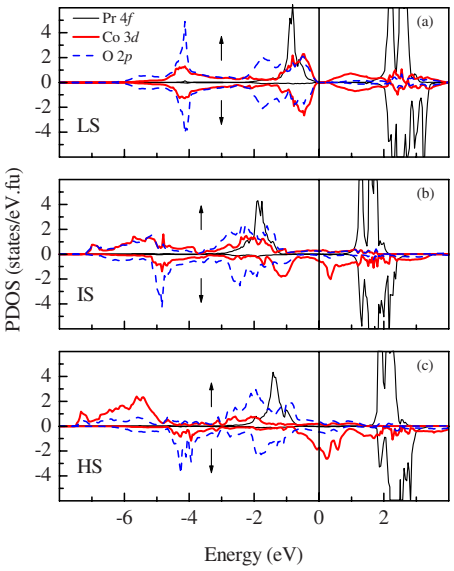

FIG. 4. (Color online) Calculated Pr $4f$ (thin solid line), Co $3d$ (thick solid line), and O $2p$ (dashed line) partial density of states corresponding to (a) LS, (b) IS, and (c) HS configurations using GGA+U method including spin-orbit coupling.

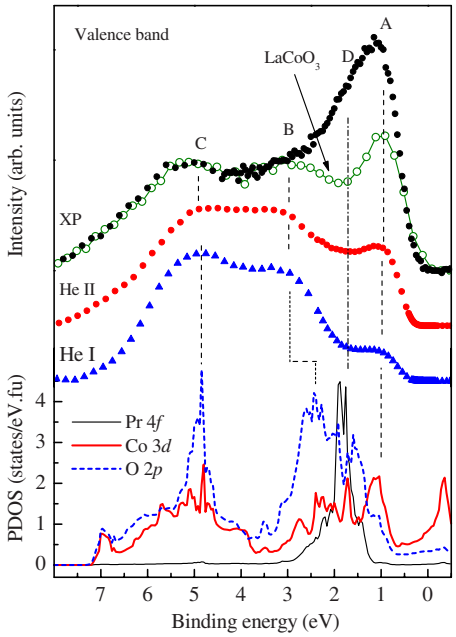

FIG. 5. (Color online) Experimental valence band spectra collected at room temperature using Al $K\alpha$, He II, and He I, radiations. The lines denote the calculated Pr $4f$ (thin solid line), Co $3d$ (thick solid line), and O $2p$ (dashed line) partial density of states corresponding to the intermediate spin configuration of a Co ion obtained from GGA+U calculation including spin-orbit coupling. Room temperature experimental valence band spectrum of $LaCoO_3$ recorded by using Al $K\alpha$ radiation is also shown by hollow circles.

increases from LS to IS by about 1 eV and further increases by about 0.3 eV in the HS state. The Co $3d$ character of the energy bands at lower energies is gradually enhanced with the increase in spin state. The Co $3d$ character of the energy bands close to ϵ_F observed in the LS state is significantly reduced in the IS state. In the HS state, the energy band with a dominant Co $3d$ character appears below −5 eV.

In Fig. 5, we show the background subtracted experimental valence band spectra of $PrCoO_3$ recorded at room temperature by using monochromatic Al $K\alpha$, He II, and He I. All the spectra show zero intensity at the Fermi level, indicating the insulating behavior of the compound. All the spectra exhibit three distinct peaks at about 1.1, 3.2, and 4.9 eV marked by A, B, and C, respectively. The Al $K\alpha$ spectrum is dominated by the intensity of peak A. This trend is reversed in the He II and He I data. Due to the matrix element effect, the photoemission cross section corresponding to various electronic states significantly changes with the change in photon energy. The relative cross section of O $2p$ states with respect to those of the Co $3d$ and Pr $4f$ states is significantly higher in ultraviolet photon energies. The Al $K\alpha$ photon energy corresponds to the reverse case. Thus, the large intensity of features B and C in the He I and He II spectra as compared to the intensity of feature A indicates that features B and C have a dominant O $2p$ character and that feature A is essentially contributed by the Co $3d$ and Pr $4f$ states. In order to investigate the energy positions of the Pr $4f$ and Co $3d$ contributions, we compare the Al $K\alpha$ spectrum of $PrCoO_3$ with that of $LaCoO_3$. Clearly, the intensity around 1 eV has a dominant Co $3d$ character. The large intensity difference observed at around 1.7 eV as marked by D in the figure corresponds to the intensities from Pr $4f$ states. This is consistent with previous studies.[31,32]

A comparison of the results in Figs. 4 and 5 indicates that the experimental results in Fig. 5 correspond closely to the results in Fig. 4(b), indicating large IS state contributions at room temperature. This is also manifested in the total energies for different spin configurations. The converged total energy of the IS configuration is found to be lower by about 1 eV/f.u. as compared that of the LS state. The HS state (S=2) could not be converged using normal procedure. This clearly suggests the stability of the intermediate spin state at room temperature as compared to other spin configurations. In order to bring out the comparison more clearly, we show the spin-integrated DOS corresponding to the IS state in Fig. 5. Evidently, the character of various features and their energy positions observed in the calculated DOS are very close to the experimental results. The experimental O $2p$ nonbonding band appears at a slightly higher binding energy as compared to that observed in the calculated results. Such a small shift in energy position of the O $2p$ nonbonding states is often observed due to the neglect of the electron correlation effect among O $2p$ electrons.[33] It is worthy to note here that the Co $3d$ band at about 6 eV binding energy in the calculated spectra, corresponding to HS state, is not seen in the experimental spectra. This indicates that the contribution from the HS state at room temperature is not significant.

It is important to note here that although features in the DOS corresponding to the IS state provide a remarkable representation of the experimental spectra, the insulating gap observed in the experimental spectra as well as in the bulk measurements could not be captured in our calculations for these parameters. One needs to enhance the values of U unrealistically high to achieve such an insulating phase. In that

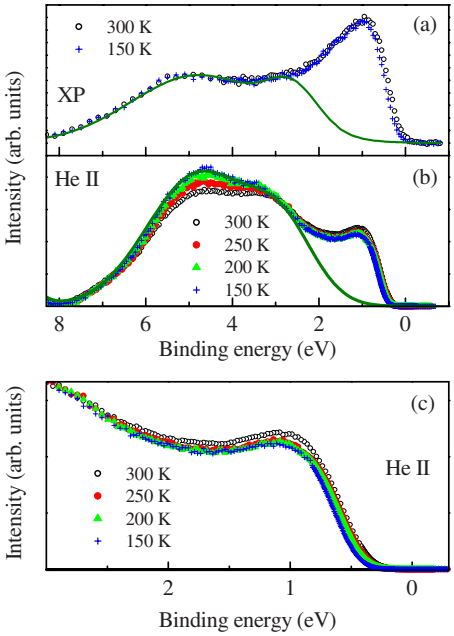

FIG. 6. (Color online) (a) Valence band spectra collected at 300 K (hollow circles) and 150 K (plus signs) using Al $K\alpha$ radiation. (b) Valence band spectra collected at 300 K (hollow circles), 250 K (solid circles), 200 K (solid triangles), and 150 K (plus signs) using He II radiation. (c) Spectra collected at 300 K (hollow circles), 250 K (solid circles), 200 K (solid triangles), and 150 K (plus signs) in the narrow region of the Fermi level using He II radiation. Solid lines in (a) and (b) indicate the contribution from O $2p$ states.

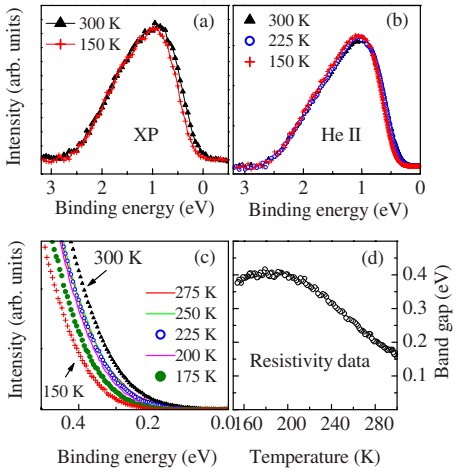

FIG. 7. (Color online) Co $3d$ and Pr $4f$ contributions extracted (a) from the XP spectra at 300 K (solid triangles) and 150 K (plus signs), and (b) from the He II spectra at 300 K (solid triangles), 225 K (hollow circles), and 150 K (plus signs). Temperature evolution of the spectra in the vicinity of the Fermi level is shown in (c) and the band gap obtained from resistivity data is shown in (d).

case, the features in the DOS will be significantly different. It is well known that orbital ordering plays an important role in determining the electronic structure of these systems. To get an insulating state, one should consider the orbital ordering in the calculations.[9] However, such considerations do not have a significant influence in the energy position of the features.

We now turn to the temperature evolution of the electronic structure. In Fig. 6, we show the valence band spectra collected at different temperatures. All the spectra are normalized by the nonbonding O $2p$ feature intensity. The XP spectra shown in Fig. 6(a) exhibit almost identical line shapes of the spectra at 300 and 150 K. The band edge appears to slightly shift toward higher binding energies. The He II spectra shown in Fig. 6(b), however, exhibit a significant change with temperature. The decrease in temperature leads to a gradual increase in intensity of the feature at around 5 eV, characterized as the bonding feature. Subsequently, the intensity of the features at around 1 eV decreases. Since the photoemission cross section corresponding to O $2p$ states is significantly enhanced in the He II photon energies, the change in Fig. 6(b) suggests a gradual enhancement of the O $2p$ character of the bonding feature with the decrease in temperature. We have expanded the near ϵ_F region of the He II spectra in Fig. 6(c) to clearly investigate the spectral changes. It is evident that the intensity at about 1 eV decreases to a lower value at 250 K as compared to the intensity at 300 K. However, a further reduction in temperature does not have a significant influence in the intensity of the feature.

From the *ab initio* results (see Fig. 4), we have observed that the increase in spin state leads to an enhancement of the Co $3d$ character at higher binding energies and that the O $2p$ contributions shift toward ϵ_F. Thus, the increase in O $2p$ character at higher binding energies with the decrease in temperature indicates that the contribution from the LS state is gradually enhanced with the decrease in temperature. These results thus provide a direct experimental evidence of the evolution of the spin state with temperature. The spectra at lower temperatures could not be measured due to the charging effect.

In order to investigate the shift of the valence band edge leading to an enhancement of the band gap with the decrease in temperature, we have extracted the distinct feature in the vicinity of the Fermi level by subtracting the features appearing at higher binding energies. The subtraction procedure is shown in Fig. 6, where the lines in the figure represent the higher binding energy features obtained by using a combination of Lorentzians convoluted by a Gaussian. The extracted features are shown in Figs. 7(a) and 7(b) for XP and He II spectra, respectively. Although these features are primarily contributed by Pr $4f$ and Co $3d$ states, the large change in photon energy (from 40.8 to 1486.6 eV), thereby different change in the photoemission cross sections of Pr $4f$ and Co $3d$ states, does not have a significant influence in the line shape of the feature. This suggests a strong mixing between the $4f$ and $3d$ contributions in this energy range.

We have expanded the spectral region in the vicinity of the band edge of the high-resolution He II spectra in Fig. 7(c). Interestingly, the band edge gradually shifts toward higher binding energies with the decrease in temperature. The shift is most significant between 300 and 275 K. In the temperature range from 275 to 200 K, the change is almost negligible and a further decrease in temperature again leads

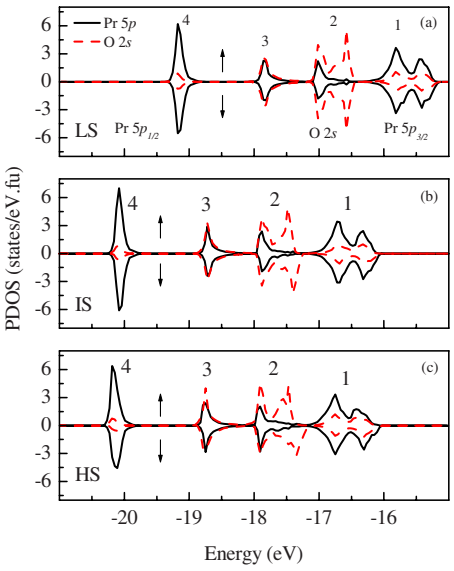

FIG. 8. (Color online) Pr $5p$ (solid line) and O $2s$ (dashed line) PDOSs calculated using the (a) LS, (b) IS, and (c) HS configurations of a Co ion.

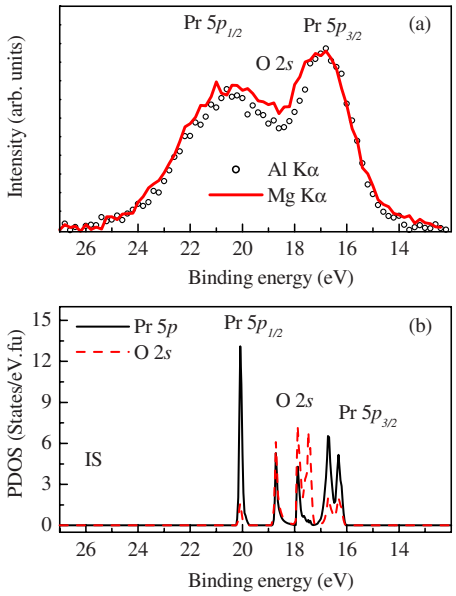

FIG. 9. (Color online) (a) Background subtracted La $5p$ and O $2s$ core level spectra collected at 300 K using Al $K\alpha$ (hollow circles) and Mg $K\alpha$ (solid lines). (b) Calculated Pr $5p$ (solid lines) and O $2s$ (dashed lines) PDOSs corresponding to the IS state configuration.

to a shift of the band edge toward higher binding energies. Such a change can be correlated to the transport data too. In Fig. 7(d), we show the activation gap calculated from the resistivity data. Interestingly, the temperature induced change of the band gap corresponds well to the shift of the band edge in Fig. 7(c).

In Fig. 8, we show the calculated majority and minority O $2s$ and Pr $5p$ PDOSs corresponding to LS, IS, and HS states. These PDOSs can be divided into four regions as marked in the figure. In the LS state, region 1 spreading over from −15.1 to −16.3 eV has a dominating Pr $5p$ character and can be attributed to the spin-orbit split Pr $5p_{3/2}$ states. Region 4 (between −18.8 and −19.3 eV) predominantly has a Pr $5p$ character, corresponding to a spin-orbit split Pr $5p_{1/2}$ state. In region 2 (from −16.4 to −17.1 eV), the contribution from O $2s$ states is most evident, and region 3 (from −17.4 to −18.0 eV) has highly mixed O $2s$ and Pr $5p$ characters. It is evident from the figures that the overall shape and spread of O $2s$ and Pr $5p$ bands remains almost the same for all the spin state configurations. However, the energy position of these bands are sensitive to the spin state of the Co ion. The whole pattern is shifted to the lower energy side by about 1.0 and 1.1 eV in the IS and HS states, respectively.

The calculated O $2s$ and Pr $5p$ PDOSs for the IS state are compared with the experimental spectra in Fig. 9. There are two distinct features in the experimental spectra centered around 16.8 and 20.6 eV. The intensity ratio of the two features are different from 1:2 expected for Pr $5p$ signals due to the overlap of the O $2s$ signal appearing in this energy range. In order to identify the character of the features, we overlap the Mg $K\alpha$ spectrum over the Al $K\alpha$ spectrum. This change in photon energy leads to a larger enhancement of the photoemission cross section of the O $2s$ states as compared to that of Pr $5p$ states.[34] A normalization by the Pr $5p_{3/2}$ peak intensity exhibits an enhancement in the energy region of 17–20 eV. This clearly indicates the presence of an O $2s$ feature in this energy region. The calculated DOS corresponding to the IS state is shown in Fig. 9(b). Evidently, the calculated DOS provides a good representation of the experimental spectra in terms of relative energy position and relative intensities.

Finally, we discuss the electronic occupancies of different orbitals and corresponding magnetic moments obtained from self-consistent calculations by considering the initial spin state of a Co ion in the LS, IS, and HS configurations. The electronic occupancies of Pr $4f$, Co t_{2g}, and Co e_g for majority and minority spin channels corresponding to LS, IS, and HS states are given in Table I. The occupancies of Pr $4f_{\uparrow}$ and Pr $4f_{\downarrow}$ are closer to 2.2 and 0.2, respectively, and insensitive

TABLE I. Electronic occupancies of Pr $4f$, Co t_{2g}, and Co e_g orbitals obtained from GGA+U calculations for LS, IS, and HS configurations of a Co ion in $PrCoO_3$.

	Pr $4f\uparrow$	Pr $4f\downarrow$	Pr $4f$	$t_{2g\uparrow}$	$e_{g\uparrow}$	$t_{2g\downarrow}$	$e_{g\downarrow}$	Pr $3d$
LS	2.18	0.21	2.39	2.77	0.59	2.77	0.56	6.69
IS	2.16	0.22	2.38	2.8	1.4	1.98	0.44	6.62
HS	2.17	0.22	2.39	2.83	1.89	1.36	0.42	6.5

TABLE II. Spin and orbital parts of the magnetic moments of Pr $4f$, Co $3d$, and O $2p$ orbitals when a Co ion is in LS, IS, and HS configurations.

	Pr $4f$ (μ_B)		Co $3d$ (μ_B)		O $2p$ (μ_B)		
	Spin	Orbital	Spin	Orbital	Spin	Orbital	μ_{eff} (μ_B)
LS	1.97	−0.47	0.03	~0	0.02	~0	2.0
IS	1.96	−0.74	1.79	0.03	0.02	0.005	3.1
HS	1.99	−0.95	2.96	0.21	0.13	0.005	4.3

to the spin state of the Co ion. However, the occupancies of $t_{2g\uparrow}$, $t_{2g\downarrow}$, $e_{g\uparrow}$, and $e_{g\downarrow}$ are very sensitive to the initial spin state configurations as expected. The total occupancy of Co $3d$ orbitals is significantly higher (~6.69) than expected for Co^{3+} (6) and gradually decreases with the increase in spin state as also observed in the case of $LaCoO_3$ in earlier studies.[30,35]

$e_{g\downarrow}$ orbitals are also found to be partially occupied; 0.56, 0.44, and 0.42 electrons in the results corresponding to LS, IS, and HS states, respectively. This is not *a priori* expected for the Co^{3+} electronic configuration. Moreover, the occupancy of the Pr $4f$ band is also greater by about 0.4 than that expected for the ionic configuration of Pr^{3+} (2.0). All these results indicate the signature of a strong hybridization among Pr $4f$, O $2p$, and Co $3d$ electronic states. This is also manifested in Fig. 3; the shapes of the Co $3d$ and O $2p$ PDOSs in the energy range of the Pr $4f$ bands are very similar to those of the Pr $4f$ PDOS.

The spin and orbital parts of the magnetic moment of Pr $4f$, Co $3d$, and O $2p$ for different spin states are given in Table II. The spin part of the magnetic moment for Pr $4f$ states is almost insensitive to the spin state of the Co ion and is closer to $2\mu_B$, suggesting a triplet state. The spin part of the magnetic moments for the Co $3d$ state, when the Co ion is in the LS, IS, and HS states, are $0.03\mu_B$, $1.79\mu_B$, and $2.96\mu_B$, respectively. Surprisingly, the orbital part of the magnetic moment for Pr $4f$ comes out to be negative and strongly depends on the spin state of the Co ion. Its magnitude increases with the increase in spin state. The negative sign indicates that the orbital and spin moments are antiparallely coupled. The orbital moment of the Co $3d$ electrons is almost zero for the LS and IS states, and for HS state, it is $0.21\mu_B$. In addition, one can also see the contribution of the spin part of the magnetic moment from O $2p$ electrons when the Co ion is in the HS state.

By using the values of magnetic moments given in Table II, one can calculate the effective magnetic moment of $PrCoO_3$. This quantity can be directly compared with susceptibility data. The calculated values obtained for the LS, IS, and HS states are about $2.0\mu_B$, $3.1\mu_B$, and $4.3\mu_B$, respectively. The effective magnetic moment estimated by fitting the magnetic susceptibility data between 100 and 150 K by using the Curie–Weiss law[6] is found to be $3.6\mu_B$. The magnetic moment depends on the electronic interaction parameters (already considered in the calculations) and various induced effects (not considered in the calculations). It is, thus, often observed that the calculated magnetic moment is underestimated in the *ab initio* results. Considering this fact, a slightly smaller value of $3.1\mu_B$ in the IS state has a good correspondence to the experimental results. However, one cannot rule out some contributions from the HS state at these temperatures, which will enhance the magnetic moment to a higher value.

IV. CONCLUSIONS

In summary, we have investigated the detailed electronic structure of $PrCoO_3$ and its temperature evolutions by using various forms of *ab initio* calculations and high-resolution photoemission spectroscopy. We observe that GGA+U calculations provide a good description of the electronic structure of this compound. Partial density of states obtained for various configurations and parameters exhibits the signature of a strong hybridization of Pr $4f$ states with Co $3d$ and O $2p$ valence electrons. In addition to the electron correlations, spin-orbit coupling plays an important role in determining the electronic structure of this compound.

The calculated Pr $4f$, Pr $5p$, Co $3d$, O $2s$, and O $2p$ partial density of states corresponding to the IS state of a Co ion provide a good representation of the experimental spectra at 300 K. The contribution from high spin state configurations appears to be negligible. Pr $5p$ and O $2s$ core level spectra could be captured reasonably well within this formalism. The decrease in temperature from 300 K leads to an enhancement of the LS contributions in the electronic structure. The band gap is gradually enhanced with the decrease in temperature as observed in the transport data.

ACKNOWLEDGMENT

S.P. is thankful to CSIR, India, for financial support.

*kbmaiti@tifr.res.in

[1] M. Imada, A. Fujimori, and Y. Tokura, Rev. Mod. Phys. **70**, 1039 (1998).
[2] R. R. Heikes, R. C. Miller, and R. Mazelsky, Physica (Amsterdam) **30**, 1600 (1964).
[3] V. G. Bhide, D. S. Rajoria, and Y. S. Reddy, Phys. Rev. Lett. **28**, 1133 (1972).
[4] S. Yamaguchi, Y. Okimoto, and Y. Tokura, Phys. Rev. B **54**, R11022 (1996).
[5] S. Yamaguchi, Y. Okimoto, H. Taniguchi, and Y. Tokura, Phys. Rev. B **53**, R2926 (1996).
[6] S. Tsubouchi, T. Kyômen, M. Itoh, and M. Oguni, Phys. Rev. B **69**, 144406 (2004).
[7] J. B. Goodenough, J. Phys. Chem. Solids **6**, 287 (1958).
[8] P. M. Raccah and J. B. Goodenough, Phys. Rev. **155**, 932 (1967).
[9] M. A. Korotin, S. Yu. Ezhov, I. V. Solovyev, V. I. Anisimov, D. I. Khomskii, and G. A. Sawatzky, Phys. Rev. B **54**, 5309 (1996).
[10] Y. Kobayashi, N. Fujiwara, S. Murata, K. Asai, and H. Yasuoka, Phys. Rev. B **62**, 410 (2000).
[11] C. Zobel, M. Kriener, D. Bruns, J. Baier, M. Grüninger, T. Lorenz, P. Reutler, and A. Revcolevschi, Phys. Rev. B **66**, 020402(R) (2002).
[12] P. G. Radaelli and S. W. Cheong, Phys. Rev. B **66**, 094408 (2002).
[13] G. Maris, Y. Ren, V. Volotchaev, C. Zobel, T. Lorenz, and T. T. M. Palstra, Phys. Rev. B **67**, 224423 (2003).
[14] V. P. Plakhty, P. J. Brown, B. Grenier, S. V. Shiryaev, S. N. Barilo, S. V. Gavrilov, and E. Ressouche, J. Phys.: Condens. Matter **18**, 3517 (2006).
[15] D. Phelan, D. Louca, S. Rosenkranz, S.-H. Lee, Y. Qiu, P. J. Chupas, R. Osborn, H. Zheng, J. F. Mitchell, J. R. D. Copley, J. L. Sarrao, and Y. Moritomo, Phys. Rev. Lett. **96**, 027201 (2006).
[16] L. Sudheendra, Md. M. Seikh, A. R. Raju, and C. Narayana, Chem. Phys. Lett. **340**, 275 (2001).
[17] J.-Q. Yan, J.-S. Zhou, and J. B. Goodenough, Phys. Rev. B **69**, 134409 (2004).
[18] R. F. Klie, J. C. Zheng, Y. Zhu, M. Varela, J. Wu, and C. Leighton, Phys. Rev. Lett. **99**, 047203 (2007).
[19] K. Knízek, Z. Jirák, J. Hejtmánek, and P. Novák, J. Phys.: Condens. Matter **18**, 3285 (2006).
[20] M. W. Haverkort, Z. Hu, J. C. Cezar, T. Burnus, H. Hartmann, M. Reuther, C. Zobel, T. Lorenz, A. Tanaka, N. B. Brookes, H. H. Hsieh, H.-J. Lin, C. T. Chen, and L. H. Tjeng, Phys. Rev. Lett. **97**, 176405 (2006).
[21] A. Podlesnyak, S. Streule, J. Mesot, M. Medarde, E. Pomjakushina, K. Conder, A. Tanaka, M. W. Haverkort, and D. I. Khomskii, Phys. Rev. Lett. **97**, 247208 (2006).
[22] M. Abbate, J. C. Fuggle, A. Fujimori, L. H. Tjeng, C. T. Chen, R. Potze, G. A. Sawatzky, H. Eisaki, and S. Uchida, Phys. Rev. B **47**, 16124 (1993).
[23] S. R. Barman and D. D. Sarma, Phys. Rev. B **49**, 13979 (1994).
[24] S. K. Pandey, R. Bindu, Pramod Bhatt, S. M. Chaudhari, and A. V. Pimpale, Physica B **365**, 47 (2005).
[25] S. Y. Savrasov, Phys. Rev. B **54**, 16470 (1996); Z. Kristallogr. **220**, 555 (2005).
[26] S. H. Vosko, L. Wilk, and M. Nusair, Can. J. Phys. **58**, 1200 (1980).
[27] J. P. Perdew, K. Burke, and M. Ernzerhof, Phys. Rev. Lett. **77**, 3865 (1996).
[28] K. Maiti, D. D. Sarma, T. Mizokawa, and A. Fujimori, Phys. Rev. B **57**, 1572 (1998); Europhys. Lett. **37**, 359 (1997).
[29] K. Maiti, D. D. Sarma, M. J. Rozenberg, I. H. Inoue, H. Makino, O. Goto, M. Pedio, and R. Cimino, Europhys. Lett. **55**, 246 (2001); A. E. Bocquet, T. Mizokawa, K. Morikawa, A. Fujimori, S. R. Barman, K. Maiti, D. D. Sarma, Y. Tokura, and M. Onoda, Phys. Rev. B **53**, 1161 (1996).
[30] S. K. Pandey, Ashwani Kumar, S. Patil, V. R. R. Medicherla, R. S. Singh, K. Maiti, D. Prabhakaran, A. T. Boothroyd, and A. V. Pimpale, Phys. Rev. B **77**, 045123 (2008).
[31] S. K. Pandey, Ashwani Kumar, S. M. Chaudhari, and A. V. Pimpale, J. Phys.: Condens. Matter **18**, 1313 (2006).
[32] T. Saitoh, D. Ishii, A. Hachimura, M. Hirose, T. S. Naing, Y. Kobayashi, K. Asai, M. Nakatake, M. Higashiguchi, K. Shimada, H. Namatame, and M. Taniguchi, J. Magn. Magn. Mater. **310**, 981 (2007).
[33] D. D. Sarma, N. Shanthi, S. R. Barman, N. Hamada, H. Sawada, and K. Terakura, Phys. Rev. Lett. **75**, 1126 (1995).
[34] J. J. Yeh and I. Lindau, At. Data Nucl. Data Tables **32**, 1 1985.
[35] T. Saitoh, T. Mizokawa, A. Fujimori, M. Abbate, Y. Takeda, and M. Takano, Phys. Rev. B **55**, 4257 (1997).